Orientational Behavior of Single Molecules in Molecular Sieves: A Study of Oxazine Dyes in $AlPO_4$-5 Crystals

Christian Seebacher, Christian Hellriegel, and Christoph Bräuchle*

Department Chemie, Ludwig-Maximilians-Universität München, Butenandtstrasse 11 (Haus E), D-81377 München, Germany

Matthias Ganschow and Dieter Wöhrle

Institut für Organische und Makromolekulare Chemie, Universität Bremen, Postfach 330440, D-28334 Bremen, Germany

Received: November 11, 2002; In Final Form: March 27, 2003

Three differently sized oxazine dye molecules, oxazine-1, oxazine-170, and oxazine-750, with molecular widths of 0.85, 1.0, and 1.1 nm, respectively, have been built into the one-dimensional pores of $AlPO_4$-5 with a pore diameter of 0.73 nm during a template assisted synthesis. There is evidence that a deformed oxazine-1 molecule can tightly fit into these pores, whereas the larger molecules produce defect sites. The orientations of the used dyes were measured with polarization dependent fluorescence confocal microscopy. Ensemble measurements on the samples containing the oxazine dyes in high concentration reveal a preferential orientation of the molecules along the main axis of the crystal. However, the ensemble measurements cannot reveal the orientational distribution function of tilt angles. Therefore, this distribution function was obtained by measuring the orientations of many individual molecules using single molecule spectroscopy. The thinnest molecule, oxazine-1, shows a Gaussian type distribution of tilt angles with a half width at half-maximum of $\xi = 18°$. The medium sized oxazine-170 shows a broader Gaussian tilt function with $\xi = 48°$, whereas the broadest molecule oxazine-750 does not show a preferential orientation. These results clearly show that there is a structure directing influence of the host on the guest molecules in dependence of their size, even if the molecule is larger than the pore size. Additionally, distinct orientational jumps of individual oxazine-1 molecules were observed. Dynamic events such as these cannot be revealed by conventional ensemble spectroscopy.

1. Introduction

Composite materials, in which guest molecules are incorporated into nanostructured solid host matrixes, such as molecular sieves, constitute a promising class of materials,[1−3] most particularly in the context of functional materials. While an interesting range of applications has already been realized on the basis of such materials, for example, micrometer sized dye lasers,[4] chemical sensors,[5,6] and nonlinear optical materials,[7] the characterization thereof is often incomplete. We have recently shown that confocal microscopy poses an expeditious tool for the characterization of such materials regarding the detection of defect structures.[8] We have also recently published an account on the characterization of the translational diffusion of guest molecules in a mesoporous molecular sieve using single molecule spectroscopy (SMS).[9] In this article we will present a further characterization regarding the orientational distribution of single molecules in a molecular sieve, using a single molecule sensitive confocal microscope. In the past decade SMS has evolved to become a fundamental tool in molecular physics.[10−17] Although one of the main interests of SMS-based research currently focuses on biophysical problems,[18−22] it is also clear that it can be used as a powerful method in material science.[23−27] The main advantage of SMS lies in the elimination of ensemble averaging, thus giving direct access to the distribution of a studied property.[15] Additionally, it allows us to directly observe mechanistic processes, which are often hidden by the ensemble averaging in conventional spectroscopic methods.

The most basic property of host−guest materials, such as molecules incorporated in molecular sieves, is their structural organization. The orientation of the incorporated guest molecules being one of the structural aspects of fundamental importance. For example, the non-centrosymmetric orientation of the guest molecules is crucial for the function of nonlinear optical devices based on these materials.[7] As another example, the orientation of the guest molecules plays an important role in the transfer of electronic excitation energy[28] within a host−guest structure. The obvious questions regarding the orientation of molecules in such a host−guest material are as follows:[29] How well-defined is the orientation of the molecules? How can this be measured?

A solid sample containing molecules with one preferential orientation will be optically anisotropic. This anisotropy can be inferred by polarization dependent microscopy. In the case of fluorescent dye molecules, the detected fluorescence intensity varies with the polarization plane of the excitation light, because the transition dipole moment is a vector.

The orientation of single molecules can be obtained in the following two ways: Either the fluorescence intensity is recorded as a function of the rotation of the excitation polarization or the fluorescence emission is analyzed in two perpendicular polarization channels, after excitation with circularly polarized light.[30] In the first case the orientation of the absorption transition dipole moment is determined, whereas in the second case the emission transition dipole moment is obtained. With the possibility to perform SMS in host−guest materials, a whole

10.1021/jp027434w CCC: $25.00
Published on Web 05/20/2003

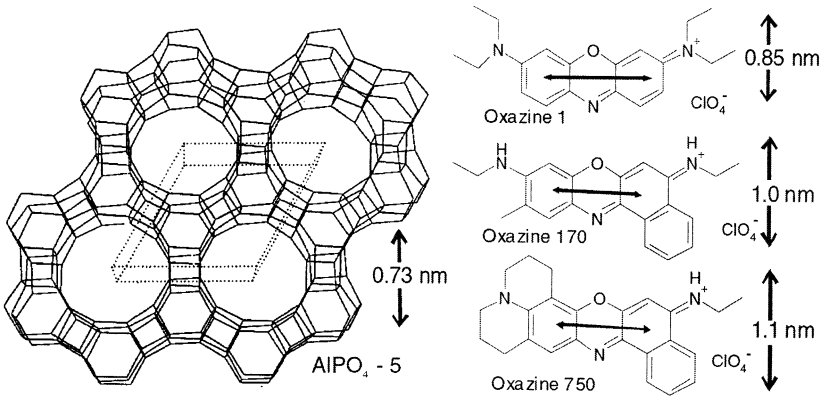

Figure 1. Structure of $AlPO_4$-5 with pore size and chemical structures of the used oxazine dyes. The arrows beside the structures represent the estimated sizes of the pore and of the molecules, calculated from the bond lengths[34] and van der Waals radii.[35] The arrows inside the chemical formula indicate the calculated orientation of the transition dipole moment for the first electronic transition of the dyes.

new wealth of data can be obtained for these materials. One should bear in mind that in ensemble measurements, in contrast to single molecule experiments, only an average value for the orientational distribution is obtained. Therefore, these measurements cannot reveal the orientational distribution function itself. Additionally, in SMS it is also possible to detect the dynamic orientational behavior of single molecules, which would otherwise be hidden in the ensemble average.

SMS investigations are best carried out with molecules that fluoresce in the red part of the visible spectrum, because of the lower background signal, due to less scattering and less autofluorescence. Photostability is another crucial requirement for these measurements. Dye molecules with these properties are commonly large and have a rigid chromophore structure.[15] Since the pore size of crystalline molecular sieves is relatively small, the width of the fluorescent guest molecules should be chosen to be as small as possible. The oxazine dyes provide a compromise between small size and suitable fluorescence properties for the SMS experiments. On the other hand, an appropriate host material should have channels that are wide enough to incorporate the guest molecules. In addition, it should allow the inclusion of the dye molecules during synthesis under soft reaction conditions to prevent the dyes from degradation. Furthermore, the crystal size has to be big enough to allow optical microscopy inside the crystal. The $AlPO_4$-5 material meets all these requirements quite well. The three different oxazine dyes chosen are depicted in Figure 1 together with the pore structure of the $AlPO_4$-5 material. The dyes have been included during the template assisted synthesis. From the width of the dye molecules and the pores, it is obvious that oxazine-170 and oxazine-750 will not easily fit into the pores but will induce defects instead. However, these will be local internal defects in the channels and will not affect the morphology of the crystal. In the case of oxazine-1 molecules, however, the ethyl groups at both amino ends can be deformed to some extent and, therefore, allow the molecule to fit into the channels, as diffusion experiments with this molecule suggest.[31] In addition, we cannot exclude that oxazine-1 also forms defect sites generated during the template synthesis. In all cases it is highly interesting to learn if, and to what extent, a preferential orientation of the molecules is present. Particularly interesting is the question of the structure directing influence of the host on the guest, even if the width of the guest molecules exceeds the pore size.

In this article we will present the data for the orientational distribution of the three different oxazine dye molecules shown in Figure 1 incorporated as guests in an $AlPO_4$-5 molecular sieve. Such data were obtained by SMS for the first time. With this method, the distribution function of the orientation of molecules in a structured host is revealed in the most rigorous way. We will discuss these results with regard to the structure directing influence of the host on the guest molecules. Additionally, we could observe the orientational dynamics of some individual oxazine molecules, that is, the jumping between several distinct orientations. Due to the size of the molecules, this has to occur in defect sites of the host material. We will compare the information gained from the SMS measurements with the data gathered from conventional ensemble measurements, thus showing how SMS allows a more thorough description of the inspected material.

2. Experimental Section

The $AlPO_4$-5 crystals containing the oxazine dyes were investigated with a modified inverted confocal laser scan microscope (ZEISS LSM 410). The birefringence of the micrometer-sized crystals is negligible.[32] An oil immersion objective with a high numerical aperture (ZEISS 40 $\times$ 1.3 oil) was used to achieve high spatial resolution and high light detection efficiency. The built-in He−Ne laser with a wavelength of 633 nm was used for the excitation of the fluorescent dyes. The fluorescence light was separated from the laser light using a combination of filters consisting of a dichroic mirror (Q640LP AHF Analysentechnik) and a combination of two fluorescence filters (633 nm Notch Kaiser; HQ720/150 AHF Analysentechnik). The fluorescence is detected outside the microscope with a single photon counting avalanche photodiode (EG&G SPCM-AQ 141). The electronic signal width of the photodiode is adjusted with a variable monoflop circuit and redirected to one analog input channel of the microscope. The samples were embedded in PMMA to obtain a better matching of the refractive indices. A more detailed description of the setup used can be found in a previous publication.[9] The acquired fluorescence information comes from the confocal volume element, which is an ellipsoid of approximately 300 nm diameter in the focal plane and 900 nm along the optical axis. One relevant device for the measurement of the orientation consists of a rotating, broad band $\lambda/2$ plate, which is placed just before the objective barrel to avoid disturbing polarization effects from the dichroic mirror. This continuously rotating plate is used to modulate the polarization plane of the excitation light. The modulation is monitored by recording the transmitted excitation light intensity behind the sample and after a polarization filter. A schematic picture of this part of the setup is shown in Figure 2a. For orientational measurements two modulation curves are

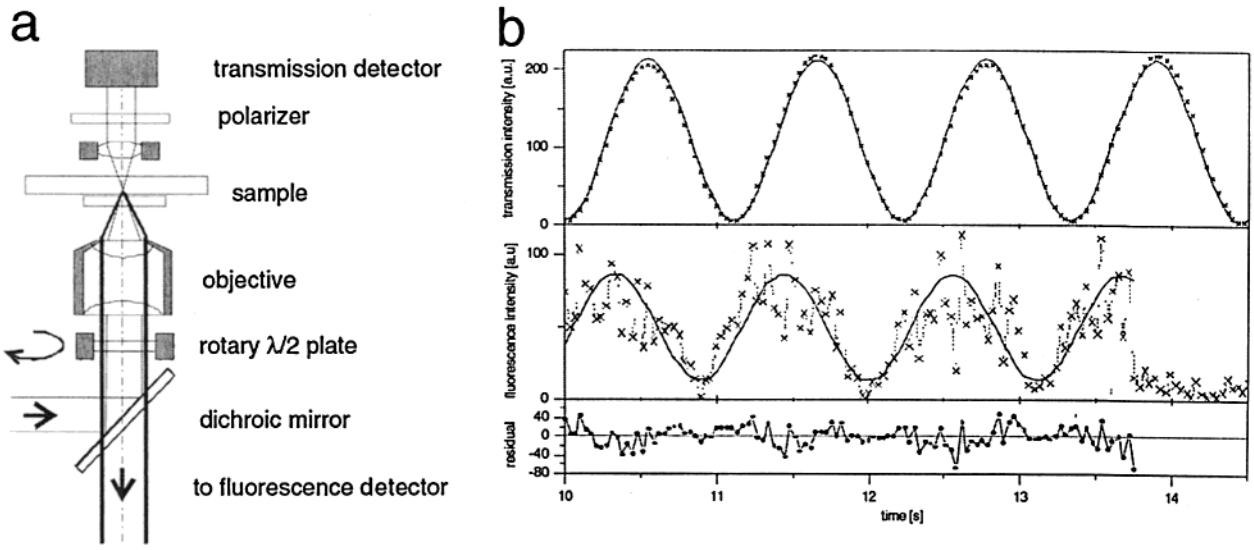

Figure 2. (a) Schematic representation of the used experimental setup. Parallel laser light is routed into the microscope objective by a dichroic mirror. Just before the objective barrel a rotary $\lambda/2$ plate rotates the polarization plane of the excitation light. The transmitted laser light is analyzed by a polarizing filter and detected. Fluorescence from the sample is collected by the objective and passes the $\lambda/2$ plate and the dichroic mirror to the fluorescence detector. (b) The resulting curve for the polarization dependent measurements (here, for a single molecule). The upper graph originates from the modulated transmission light after the polarizer. The lower graph results from the modulated fluorescence intensity of the molecule, as recorded by the fluorescence detector (note the one-step photobleaching at ~13.8 s). The smooth curves are the cosine-square fit through the data according to eq 2.

recorded simultaneously in dependence of the rotation of the $\lambda/2$ plate. The upper graph in Figure 2b shows the modulation of the transmission intensity of the excitation light wave, which is detected behind the polarizer. The lower graph shows the modulated fluorescence intensity which is detected simultaneously at the fluorescence detector—in this case of a single molecule. A more detailed description of the evaluation of these curves will be given in the next section.

The dye loaded $AlPO_4$-5 crystals are synthesized according to the method described in the literature,[33] which was modified in order to include the dye molecules. The $AlPO_4$-5 molecular sieve was synthesized using pseudoboehmite (Plural SB, ~75% Al_2O_3, Condea Chemie), orthophosphoric acid (H_3PO_4, 85 wt %, p.a., Merck), tripropylamine (Pr_3N, Merck), and deionized water as source materials. The batch composition was $1Al_2O_3/1P_2O_5/2Pr_3N/150H_2O$. Al_2O_3 (4.12 g) was added to 6.92 g of H_3PO_4 in 20 g of H_2O under strong mechanical stirring. After 2 min a further 61 g of H_2O was added. After 5 min a uniform gel was formed, and then 8.6 g of tripropylamine was slowly added under stirring. The agitated gel aged for 15 h at room temperature. Parallel to this procedure, a stock solution of 10^{-5} mol of oxazine dye in ethanol was prepared. For the encapsulation of the respective oxazine dye, this solution was further diluted in steps of 10-fold dilution, and 1 mL of that solution was mixed with 25 g of the gel at the end of the aging period. The gel was filled in a 100 mL Teflon autoclave, sealed and deposited in the microwave oven (MLS 1200 Mega, Milestone). The synthesis batch was quickly heated (4.5 °C/s, 1000 W) to 155 °C within 1 min and kept at the required temperature for 15 min. Then the autoclave was quench-cooled with iced water. The crystalline product was rinsed with water and with ethanol and then dried overnight at 80 °C. Around 0.6−1.0 g of product were obtained. Note that water and the template—tripropylamine—are also present in the pores after the synthesis of $AlPO_4$-5. The crystal structure of the samples was determined by X-ray diffraction (Philips PW-1050 X'Change, Cu $K_{\alpha 1}$, Bragg−Brentano geometry, secondary monochromator), and its morphology was visualized by scanning electron microscopy (ISI-100B, 15 kV). The results show that the crystal structure and the morphology of the $AlPO_4$-5 are not affected by the inclusion of the dye molecules, in comparison to the case of control batches lacking dye.

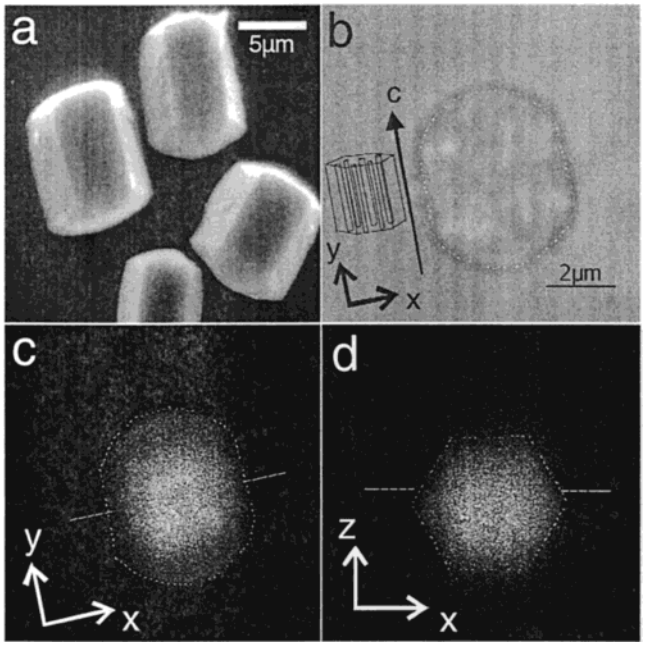

Figure 3. (a) SEM image of the $AlPO_4$-5 crystals. (b) The transmission image showing an $AlPO_4$-5 crystal lying with the *c* axis (axis of the pores) in the focal plane of the microscope (cf. the schematic inset). This crystal contains oxazine-1 in high concentration (~10^{-5} mmol/g employed in synthesis). (c) The corresponding confocal fluorescence image of the same crystal as in part b viewed from the same perspective. (d) Confocal fluorescence cross-section perpendicular to the *xy*-plane of the same crystal. The dashed lines through the crystal in the last two figures denote the respective planes of observation in parts c and d.

The used $AlPO_4$-5 crystals look like micrometer sized hexagonal barrels with bulges on both ends. Figure 3a shows an SEM image of these crystals. The unidimensional pores are perpendicular to the hexagonal sections of the crystals, that is,

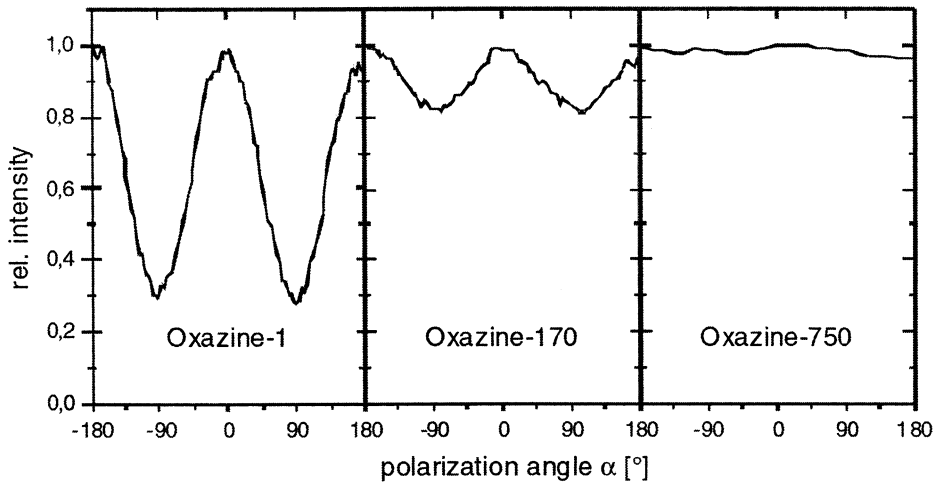

Figure 4. Experimental data for the modulation of the fluorescence intensity depending on the polarization angle α of the excitation light. The data are obtained in ensemble measurements for oxazine-1, oxazine-170, and oxazine-750 in high dye concentration ($\sim 10^{-5}$ mmol/g employed in synthesis).

parallel to the straight sides of the barrel. The images in Figure 3b−d show one $AlPO_4$-5 crystal containing oxazine-1 in high concentration, as observed with the confocal microscope in transmission (b) and fluorescence (c and d) modes. To evaluate the dye orientations with respect to the pore axis, only those crystals with pores lying in the focal plane of the microscope are used.

3. Results and Discussion

Experiments have been carried out with probes containing oxazine dyes in high (ensemble) and in ultralow concentrations (single molecules). This section will be subdivided into two parts to stress the differences between SMS and conventional ensemble spectroscopy.

Ensemble Measurements. The three oxazine-$AlPO_4$-5 samples, with concentrations typical for ensemble measurements (on the order of 10^{-5} mmol/g), were inspected with polarization dependent confocal microscopy. The confocal detection volume was always kept inside the crystal, to prevent a disturbing influence from molecules adsorbed on the outer surface of the crystal. The measurements were performed in the same manner as described for the single molecule measurements (see below). Figure 4 shows the relative fluorescence intensity of the three samples used, with respect to the angle α of the polarization plane of the excitation light relative to the crystal axis. The orientation of the crystal axis, which corresponds to the orientation of the pores, is determined from transmission images. This orientation is used as a reference and is set to 0°. A cosine-square modulation of the fluorescence intensity is observed. In the following, the ratio between the intensity at 90° ($I_{90°}$) and the intensity at 0° ($I_{0°}$) of the polarization plane of the excitation light will be termed the modulation loss. It can be directly read off the graph at the value $\alpha = \pm 90°$, because the curves are normalized. In principle, the modulation loss would be zero for perfectly aligned molecules (that is, the modulation would be maximal). We note that the modulation loss increases on going from the most narrow molecule used, oxazine-1 ($I_{90°}/I_{0°} = 0.29$), to the next broader molecule, oxazine-170 ($I_{90°}/I_{0°} = 0.81$). The modulation vanishes completely for the sample containing the broadest of all the molecules used, oxazine-750 ($I_{90°}/I_{0°}$ close to unity).

The physical or geometrical reason for this increasing modulation loss is explained by an increasing misalignment of the molecules relative to the crystal axis, similar to the exemplary behaviors depicted in the insets of Figure 5d. To characterize this misalignment, the characteristic angular distribution function for the tilt angle of the transition dipole moment with respect to the crystal axis and the width of this distribution function should be obtained. However, except for the trivial solution, where all molecules are aligned perfectly, a distribution function cannot be obtained from one value (namely the modulation loss) alone. Therefore, the assumption of a distribution model is necessary to obtain the angular distribution function from such ensemble measurements.

To obtain this distribution from the ensemble measurements, we propose three reasonable, axially symmetric models (cf. Figure 5). In the first model the transition dipole moments are tilted at a constant angle ξ from the main crystal axis, leading to a uniform distribution on a cone surface (Figure 5a). That distribution would make sense if the dyes were incorporated at a well-defined tilt angle ξ within the crystal structure. In the second model the transition dipole moments are distributed uniformly below a constant angle ξ, leading to a uniform distribution in a cone volume (Figure 5b). That model would reflect the possibility that the molecules are incorporated in well-defined voids which are larger than the molecule. The third model assumes a Gaussian angular distribution with a characteristic half-width at half-maximum ξ (Figure 5c). In that model the pore structure could have a directing influence, but the defect size and orientation would otherwise be random. All these models are characterized by their half apex angle ξ.

To calculate the expected fluorescence intensity at a polarization angle α of the incident light wave for these models, the following procedure was used: For an axially symmetric system the angular distribution is a function of the azimuth-angle θ. This distribution is depicted for all three cases in the upper images in Figure 5a−c. From this distribution a three-dimensional representation is obtained, as depicted in the middle images of Figure 5a−c. This finally leads to a two-dimensional projection of this distribution into the focal plane of the microscope, which is the plane of experimental observation. These projections are depicted in the lower graphs in Figure 5a−c. From these projections the fluorescence intensity $I(\xi,\alpha)$ as a function of the model characterized by ξ and the polarization angle α of the incident light-wave can be calculated according to eq 1:

$$I(\xi,\alpha) = \int D_{2D}(\theta,\xi) \cos^2(\theta - \alpha)\, d\theta \qquad (1)$$

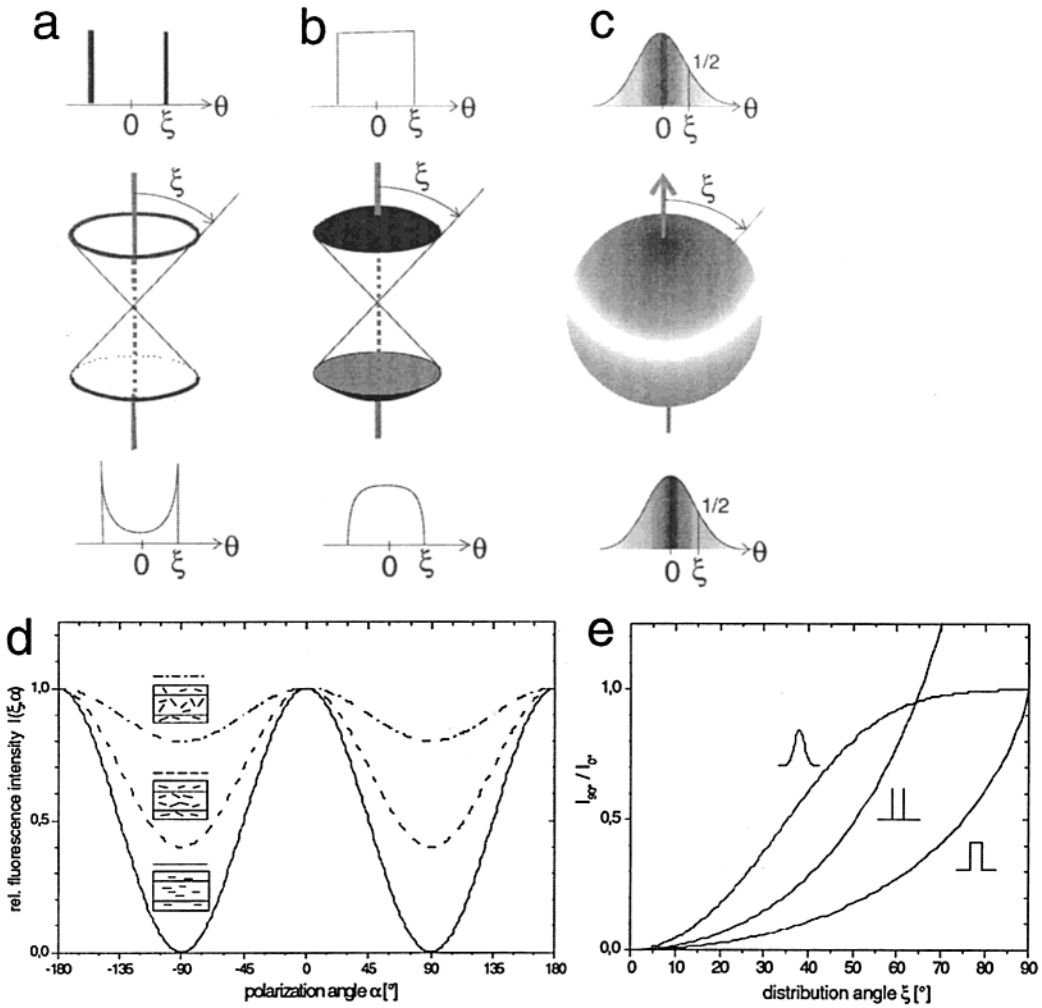

Figure 5. Three different models for orientational guest distributions in an axially symmetric host system. The cone surface model is shown in part a whereas the cone volume model and Gaussian model are shown in parts b and c, respectively. In all models the top row shows the angular distribution, the middle row represents the three-dimensional distribution, and the bottom row shows the two-dimensional projection of the respective distribution of the transition dipole moments into the plane of observation. θ is the azimuth angle, and ξ is the half apex angle characterizing each distribution. For details see text. (d) Relative fluorescence intensity $I(\xi,\alpha)$ as a function of the polarization angle α according to eq 2. The insets show three different degrees of order for the corresponding polarization curves. (e) Calculated modulation loss ($I_{90°}/I_{0°}$) versus the half apex angles ξ for the three different distribution models.

Here, $D_{2D}(\theta,\xi)$ is the two-dimensional projection of the angular distribution of the transition dipole moments into the focal plane, and the term $\cos^2(\theta - \alpha)$ describes the amount of projected in-plane transition dipole moments matching with the excitation light polarization at α. Taking the integral over all in-plane angles θ yields the total intensity for an excitation polarization plane α. This function is plotted for three different distribution widths ξ, in dependence of the polarization angle α in Figure 5d. The three curves are characterized by their modulation loss $I_{90°}/I_{0°}$. This modulation loss can be plotted as a function of the distribution width ξ, for the three different models, as depicted in Figure 5e. Here it becomes apparent that the same modulation loss can originate from different distribution functions and widths. For example, the middle curve in Figure 5d has a modulation loss $I_{90°}/I_{0°}$ of 0.4 and can result from a half apex angle ξ of 31° in the Gaussian distribution model (Figure 5c), 46° in the cone surface model (Figure 5a), and 70° in the cone volume model (Figure 5b). It is obvious that these half apex angles ξ describe very different orientations of molecules within the host structure.

The following values can be obtained from the ensemble measurements in Figure 4 of oxazine-1 and oxazine-170 in $AlPO_4$-5, respectively: Gaussian distribution $\xi_{G,ox1} = 26°$ and $\xi_{G,ox170} = 51°$, cone surface distribution $\xi_{S,ox1} = 40°$ and $\xi_{S,ox170} = 61°$, and cone volume distribution $\xi_{V,ox1} = 61°$ and $\xi_{V,ox170} = 86°$. Furthermore, it is worth noting that even the sample with the oxazine-750 molecules could show a well-defined angular distribution even though there is no modulation. That would be the case for the cone surface distribution at 65.3°, which results in a complete modulation loss with $I_{90°}/I_{0°} = 1$ (cf. Figure 5e). Summarizing, there is no way to decide which orientational distribution function is present from an ensemble measurement of the fluorescence intensity $I(\xi,\alpha)$ as a function of the polarization angle α. And as a result of that, the true distribution width ξ cannot be inferred. This is the point where SMS measurements become essential.

Single Molecule Measurements. In contrast to the case of the ensemble measurements, the distribution is revealed directly by reconstructing the ensemble from each single molecule orientation. The measurements at the level of single molecules are carried out with crystals containing oxazine dyes in ultralow concentrations (below 10^{-8} mmol/g employed dye concentration in the respective synthesis batches). At this level of dilution the fluorescence images of the samples show bright diffraction limited spots in the inner part of the crystal, as seen in the lower part of Figure 6a. It is well-known that a digital on/off behavior

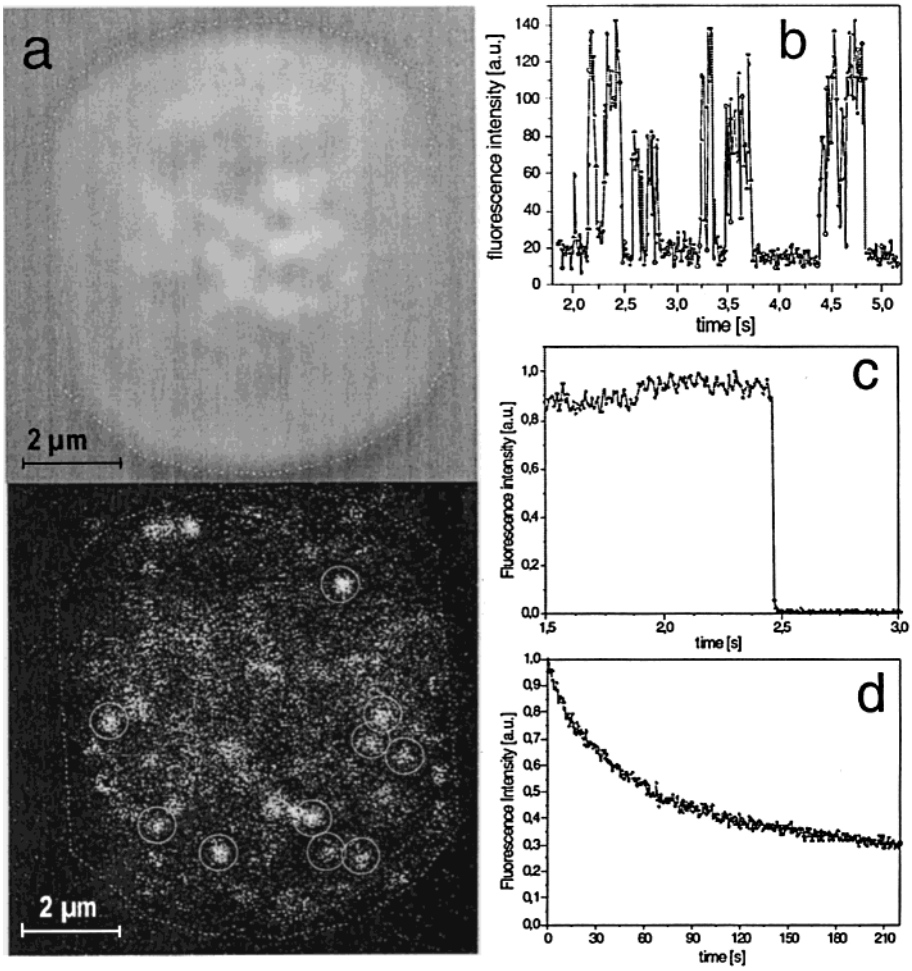

Figure 6. (a) Transmission and confocal fluorescence image of an $AlPO_4$-5 crystal containing oxazine-1 in ultralow concentration (10^{-9} mmol/g employed in synthesis). In the lower image the circles indicate the diffraction limited patterns of the fluorescence of single molecules. Part b shows the blinking of a single molecule, and part c the digital bleaching behavior. Part d is an ensemble measurement and shows the continuous photobleaching decay of a higher concentrated sample.

of the fluorescence intensity with time denotes the presence of single molecules. The on/off blinking behavior and the one-step photobleaching are seen in Figure 6b and c. In contrast, measurements at high concentrations yield a continuous fluorescence intensity decay (Figure 6d), which is the sum of many individual photobleaching steps at different times. These results prove that we can work at the level of single molecules with our confocal setup and the samples used here.

To obtain the orientation of the single molecules, their fluorescence intensity is recorded in dependence of the polarization angle α of the excitation light.[30] In this measurement an intensity maximum is expected when the polarization plane of the excitation light is parallel to the transition dipole moment of the molecule, and a minimum when it is orthogonal to it. Figure 2b shows a transmission and fluorescence curve for a single oxazine-1 molecule in $AlPO_4$-5. Both signals are described according to a cosine-squared behavior (eq 2) with the same frequency ω, which results from the rotation of the $\lambda/2$ plate, and with their respective phases ϕ (the amplitude A varies with every measurement and the offset c is given by the background signal in the fluorescence trace):

$$I(t) = A\cos^2(\omega t + \phi) + c \qquad (2)$$

The phase difference between the fluorescence and reference signals is equal to the angle of the transition dipole moment of the molecule relative to the orientation of the polarizer. The phases are obtained by fitting the measured data with eq 2. Long time traces with good signal-to-noise ratios can yield an accuracy below 1°. The absolute angles are then evaluated against the crystal main axis, which in its turn is determined from transmission images with an accuracy of ∼1−2°. Figure 7a shows the results for a typical crystal containing oxazine-1. The orientational behavior of four molecules could be observed: Three of them show a fixed orientation with tilt angles of 10°, −10°, and 15° relative to the crystal axis (equivalent to the pore orientation), whereas the fourth is observed during an orientational jump from −29° to 49.5°. This jump is obvious from the fluorescence modulation curve shown in Figure 7b. It occurs after 5.8 s of observation. Finally, the molecule photobleaches at 6.7 s.

Every crystal contains about 10 molecules that can be evaluated. Typically about five molecules bleach too fast for their angle to be determined. In a few cases the molecules are too close to the crystal edge. Such molecules are excluded from the evaluation, as they could be adsorbed on the outer surface of the crystal. After evaluating 50−60 orientations against the crystals' main axes, a histogram for each sample can be generated and the distribution function visualized. In Figure 8 the histograms and the individual absolute angles with their respective error bars are depicted. The use of absolute units is possible, because of the axial symmetry of the host material.

As a first important result, we note that the distribution form

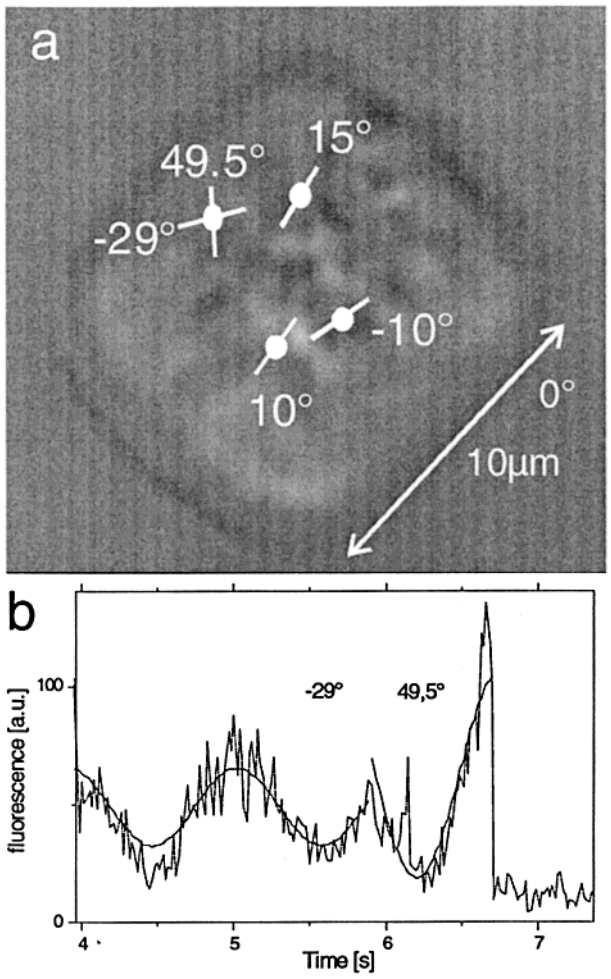

Figure 7. (a) Orientations of four different oxazine-1 molecules in $AlPO_4$-5 relative to the pore axis. The position of the molecules is indicated by the dots and the orientation by the dashes on top of a transmission image of the crystal. In one case a orientational jump during the measurement from −29° to 49.5° was observed. (b) The orientational jump as seen in the polarization modulated fluorescence intensity as a function of time.

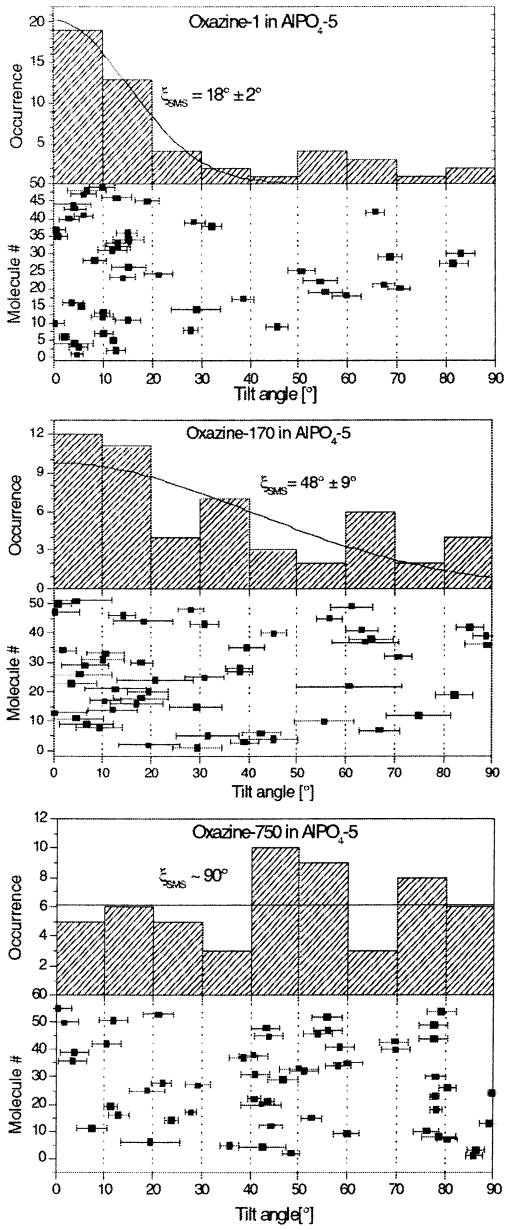

Figure 8. Distributions of the tilt angle of single oxazine dye molecules in $AlPO_4$-5 for the three systems oxazine-1, oxazine-170, and oxazine-750. The tilt angle represents the transition dipole orientation relative to the pore axis. In the upper part of each representation histograms are shown, which were generated from the single molecule orientations depicted below. Error bars are given. In the cases of oxazine-1 and -170, the half apex angles ξ_{SMS} were obtained from the histograms by a Gaussian fit. In the case of oxazine-750, no preferential orientation is observed.

shows a Gaussian-like profile, thus excluding the two cone models mentioned before. Under the assumption of a single Gaussian distribution, the half apex angles are determined to be $\xi_{SMS} = 18°$ for oxazine-1 and $\xi_{SMS} = 48°$ for oxazine-170. In the case of oxazine-750 no preferential orientation is observed. A more detailed inspection of the histogram of oxazine-1 in Figure 8 may indicate the possibility of a second subpopulation of misaligned molecules with higher tilt angles. In our case the available statistics do not allow a more precise characterization. We want to note, however, that in principle single molecule measurements can reveal the full distribution function even with different subpopulations. This is not possible for ensemble measurements, which can only give an average value and are not sensitive to distributions and cannot detect subpopulations. This is an important advantage of the SMS technique over the conventional ensemble techniques.

Comparing the results of the SMS and the ensemble measurements, there is a slightly broader distribution width in the ensemble measurements in the case of oxazine-1 ($\xi_{SMS} = 18°$ against $\xi_G = 26°$). The most plausible explanation would be that the simple Gaussian model used to fit the histograms is too idealized and, therefore, does not represent the actual distribution sufficiently. This leads to an error in the analysis of the single molecule experiments as well as in the ensemble results. The correct distribution would be obtained by single molecule experiments with sufficient statistical data. Further arguments could be used to explain the broader distribution in the ensemble measurements: first, that the more concentrated samples generate a more perturbed system, leading to a broader distribution, and, second, that a tilt angle selective photobleaching could disturb the single molecule statistics. However, we do not have indications for either arguments in our measurements.

As a second important result, a comparison between the histograms in Figure 8 reveals the structure directing influence of the host on the guest molecules in dependence of their size. All of the used molecules exceed the pore diameter of 0.73 nm of $AlPO_4$-5 (cf. Figure 1). As mentioned in the Introduction,

there are two possibilities for the inclusion for oxazine-1 into the channels of $AlPO_4$-5: by deformation of the molecule or by generating defect sites in the host. Experiments on the loading of oxazine-1 into $AlPO_4$-5 by diffusion[31] indicate that the dye molecules are deformed to some extent. The results gathered in this publication clearly show that, in addition to the dye-deformation, oxazine-1 is also included in defect sites. This is indicated by the observation of molecules with higher tilt angles in the single molecule histograms and especially by the orientational jumps observed for some of the oxazine-1 molecules, with jumping angles close to 90°.

In the case of oxazine-170 the width of the molecule (∼1.0 nm) clearly exceeds the pore size. Nevertheless, in the template synthesis, the $AlPO_4$-5 host acts as a structure directing agent forcing most of the molecules to align more or less along the channels. It is obvious that the larger width of the molecule results in a broader distribution width ξ compared to that for oxazine-1. This influence of the host on the guest vanishes after the molecular width exceeds a certain maximum value, which is between 1 and 1.1 nm, as indicated by the random orientation of oxazine-750 molecules. Oxazine-750 has a molecular width of ∼1.1 nm. This influence of the host material on the guest molecules can also be observed in the ensemble measurements (Figure 4) However, many different distribution models can lead to the observed ensemble behavior. Only SMS studies enable a more profound understanding of the underlying angular distributions.

One of the most intriguing results of the SMS experiments is the observation of orientational jumps of single oxazine-1 molecules. The observed jumps take place abruptly between distinct orientations and show no "continuous" rotation of the molecules within the defect site. This is a direct consequence of distinct minima in the orientational potential surface experienced by the molecule in the defect site. Because of photobleaching we are so far unable to determine whether the jumping is light induced or thermally driven. For the same reason the energy levels of the potential surface cannot be obtained by temperature dependent measurements. It is clear, however, that in ensemble measurements such orientational jumps and the corresponding dynamics cannot be observed because of the averaging effect. Thus, SMS provides a much more detailed picture of the host−guest system, as shown here.

4. Conclusion

In conclusion, we have shown that the SMS technique allows a thorough characterization of host−guest materials. The orientational distribution of three different oxazine dyes incorporated in an $AlPO_4$-5 crystal was reconstructed from the orientations of many individual molecules. The comparison between this method and conventional ensemble studies clearly shows that the SMS approach allows a description of the dye orientational distribution at a more fundamental level, leading to the actual orientational distribution function. Furthermore, it is shown that a host system like $AlPO_4$-5 can still have a directing influence on the guest molecules, even when the sizes of these molecules exceed the diameter of the channels. There is, however, an upper size limit for this effect. In addition, the SMS technique also reveals—the otherwise hidden—rotational mobility of single molecules incorporated in defect sites of the host.

Acknowledgment. The authors acknowledge SFB 486 and the VW−Foundation.

References and Notes

(1) Moller, K.; Bein, T. *Chem. Mater.* **1998**, *10*, 2950.
(2) Schüth, F. *Chem. Unserer Zeit* **1995**, *29*, 42.
(3) Schulz-Ekloff, G.; Wöhrle, D.; van Duffel, B.; Schonheydt, R. A. *Microporous Mesoporous Mater.* **2002**, *51*, 91.
(4) Braun, I.; Ihlein, G.; Laeri, F.; Nöckel, J. U.; Schulz-Ekloff, G.; Schüth, F.; Vietze, U.; Weiss, Ö.; Wöhrle, D. *Appl. Phys. B* **2000**, *70*, 335.
(5) Meinershagen, J. L.; Bein, T. *J. Am. Chem. Soc.* **1999**, *121*, 448.
(6) Scott, R. W. J.; Yang, S. M.; Chabanis, G.; Coombs, N.; Williams, D. E.; Ozin, G. *Adv. Mater.* **2001**, *13*, 1468.
(7) Caro, J.; Marlow, F.; Wübbenhorst, M. *Adv. Mater.* **1994**, *6*, 413.
(8) Seebacher, C.; Rau, J. P.; Deeg, F. W.; Bräuchle, C.; Altmaier, S.; Jäger, R.; Behrens, P. *Adv. Mater.* **2001**, *13*, 1374.
(9) Seebacher, C.; Hellriegel, C.; Bräuchle, C.; Altmaier, S.; Behrens, P.; Müllen, K. *J. Phys. Chem. B* **2002**, *106*, 5591.
(10) Basché, T.; Bräuchle, C. *Ber. Bunsen-Ges. Phys. Chem.* **1996**, *100*, 1269.
(11) Basché, T., Moerner, W. E., Orrit, M., Wild, U. P., Eds. *Single-Molecule Optical Detection, Imaging and Spectroscopy*; VCH: Weinheim, 1997.
(12) Nie, S.; Zare, R. N. *Annu. Rev. Biophys. Biomol. Struct.* **1997**, *26*, 567.
(13) Xie, X. S.; Trautman, J. K. *Annu. Rev. Phys. Chem.* **1998**, *49*, 441.
(14) Moerner, W. E.; Orrit, M. *Science* **1999**, *283*, 1670.
(15) Tamarat, Ph.; Maali, A.; Lounis, B.; Orrit, M. *J. Phys. Chem. A* **2000**, *104*, 1.
(16) Rigler, R., Elson, E. S., Eds. *Fluorescence Correlation Spectroscopy*; Springer Series in Chemical Physics; Springer: Berlin, 2001.
(17) Moerner, W. E. *J. Phys. Chem. B* **2002**, *106*, 910.
(18) Weiss, S. *Science* **1999**, *283*, 1676.
(19) Seisenberger, G.; Ried, M. U.; Endress, T.; Büning, H.; Hallek, M.; Bräuchle, C. *Science* **2001**, *294*, 1929.
(20) Kitamura, K.; Tokunaga, M.; Iwane, A. H.; Yanagida, T. *Nature* **1999**, *397*, 129.
(21) Rigler, R.; Widengren, J. *BioScience* **1990**, *40*, 180.
(22) Kinosita, K.; Yasuda, R.; Noji, H.; Ishiwata, S.; Yoshida, M. *Cell* **1998**, *93*, 21.
(23) Gruber, A.; Dräbenstedt, A.; Tietz, C.; Fleury, L.; Wrachtrup, J.; von Borczyskowski, C. *Science* **1997**, *276*, 2012.
(24) Schuster, J.; Cichos, F.; von Borczyskowski, C. *J. Phys. Chem. A* **2002**, *106*, 5403.
(25) Deschenes, L. A.; Vanden Bout, D. A. *Science* **2001**, *292*, 255.
(26) Kulzer, F.; Kummer, S.; Matzke, R.; Bräuchle, C.; Basché, T. *Nature* **1997**, *387*, 688.
(27) Weston, K. D.; Goldner, L. S. *J. Phys. Chem. B* **2001**, *105*, 3453.
(28) Gfeller, N.; Megelski, S.; Calzaferri, G. *J. Phys. Chem. B* **1998**, *102*, 2434.
(29) Megelski, S.; Lieb, A.; Pauchard, M.; Drechsler, A.; Glaus, S.; Debus, C.; Meixner, A. J.; Calzaferri, G. *J. Phys. Chem. B* **2001**, *105*, 25−35.
(30) Ha, T.; Enderle, T.; Chemla, D. S.; Selvin, P. R.; Weiss, S. *Phys. Rev. Lett.* **1996**, *77*, 3979.
(31) Laeri, F., Schüth, F., Simon, U., Wark, M., Eds. *Host−Guest-Systems Based on Nanoporous Crystals: Synthesis, Properties and Applications*; Wiley VCH: Weinheim, in press.
(32) Striebel, C.; Hoffmann, K.; Marlow, F. *Microporous Mesoporous Mater.* **1997**, *9*, 43.
(33) Ganschow, M.; Schulz-Ekloff, G.; Wark, M.; Wendschuh-Josties, M.; Wöhrle, D. *J. Chem. Mater.* **2001**, *11*, 1823.
(34) Dewar, M. J. S.; Thiel, W. *J. Am. Chem. Soc.* **1977**, *99*, 4907.
(35) Bondi, A. *J. Phys. Chem.* **1964**, *68*, 441.